Оптический журнал

Иконика — наука об изображении

DOI:10.17586/1023-5086-2018-85-09-49-58

Определение физической нагрузки с использованием мимической активности

© 2018 Xuqiang Li, Kan Hong, Guodong Liu

Исследована возможность использования мультиспектральных изображений лиц для определения степени физической нагрузки человека. Разработанный алгоритм обработки мультиспектральных изображений был применен для анализа мимической активности лиц добровольцев без информирования последних. Алгоритмическая модель проходила верификацию для классификации исходных показателей и степени физических нагрузок. При применении алгоритма наилучшие результаты составляли 75%, что позволяет продолжить работу по его дальнейшему внедрению. Результаты опытов продемонстрировали потенциал использования мультиспектральных изображений для неинвазивного определения степени физических нагрузок человека.

Ключевые слова: *мультиспектральное изображение, физические нагрузки*

Detection of physical stress using facial muscle activity

© 2018 Xuqiang Li, Kan Hong*, Guodong Liu*

Optoelectronics and Communication Engineering Key Laboratory, Jiangxi Science and Technology Normal University, Nanchang, Jiangxi, China

**E-mail: 16451946@qq.com*

Submitted 15.03.2018

This study investigated the potential of using multispectral imaging for detecting physical stress on human being. Participants were recruited to obtain multispectral images and, a proposed facial muscle activity detection algorithm was established without background information. The algorithm model was verified with respect to physical stress ground truth, in order to classify the baseline and physical stress status. The algorithm achieved better results in the experiment with an accuracy rate of 75%, which will provide a foundation for future industrialization. Experimental results demonstrated that multispectral imaging, as a non-invasive method, has the potential to identify physical stress on humans.

Keywords: *multispectral imaging, physical stress.*

OCIS code: *100.0100*

1. INTRODUCTION

As an important physiological index, physical stress (PS) has attracted increasing concern. The influence of physical stress on human healthy and specific diseases (symptom) have been widely studied over the past decades [1–7]. In addition to its effects on health, PS is becoming increasingly important to the industry given the response of the human body to varying degrees of fatigue [8–11]. Numerous effective non-contact stress recognition methods have been proposed. These methods are based on photo-electronic imaging and provide effective information for practical applications in commercial and health departments, especially in the fields of health management, fatigue driving recognition, and sports competition. In previous studies, stress can induce a complicated chemo-electronic analysis procedure (hypothalamic-pituitary-adrenal axis) [12–13], and heart rates (HR) are typical physical stress markers. The invasive method like electrocardiography [14–15]

and functional magnetic resonance imaging [16–17] technologies are widely used in stress recognition studies. However, these methods require the impossible, that is, for participants to acquire coordination and non-contact data. Thereby, imaging-based stress recognition methods gradually received attention from the industry. The stress induced thermal signature, such as sweating [18–19], blood flow velocity [20], HR [21–22], and breathing [23] are reported, followed by the effective extraction and extensive research on physiological parameters of the human body [23–26]. Facial features can be simply acquired by imaging technology and basically do not require human cooperation. This method is consistent with non-contact and non-intervention trends in technology. Various face imaging recognition methods that are specific to PS are also predominant [27–33]. For example, the eye blink rate and duration of eye closure were employed for detection of fatigue occurrence due to sleep deprivation or directed attention [34–36]. In addition to these features, head pose and yawning behavior in facial video is also used [37–38]. Moreover, head-motion (shaking) behaviors due to fatigue in video were captured by a webcam [39–40]. However, no progress has been made in directly associating facial imprint signals with stress markers, though we successfully extracted weak thermal facial signals for this purpose [41–42].

In contrast to thermal imaging and other imaging methods influenced by external temperature and environmental factors, hyperspectral imaging technology has been given increased attention in the field of biomedical information in recent years. This technology combines traditional imaging and spectral technology and simultaneously acquires the spatial and spectral information of an object to determine the material characteristics of this object. Hyperspectral imaging has been widely used in various fields, such as food, agriculture, medicine, geography, and archaeology [43–48]. Figure 1 illustrates a hyperspectral image of a human face. The image shows that a hyperspectral image cube contains hundreds or even thousands of narrow band image information. Images of the same person's face in varying wavelengths can provide effective information for extracting physiological parameters. Prior to this extraction, we have successfully used the hyperspectral imaging system in extracting the psychological information of a face and obtain the emotional stress status [49–51]. However, the frame rate of hyperspectral imaging technology is low, thereby making the achievement of real-time images and extraction of real-time stress status infeasible. The time allocation for extracting facial information can be up to several minutes at a time; this duration seriously affects the real-time and reliability of the algorithm. In this study, we will use a high-frame-rate multispectral imaging (MSI) system to detect PS in the human body.

Although there are many ways to detect changes in physical stress by imaging technology, the following problems may occur in practice: (1) Real-time signal denoising method is not perfect; (2) the selection of region of interest (ROI) is immature and random. The existing research results show that a single ROI signal on face cannot realize correlation with a single emotion [52]. (3) The identification of physical stress still requires baseline data, and some recognized physical stress markers are no exception. For example, it is necessary to determine the

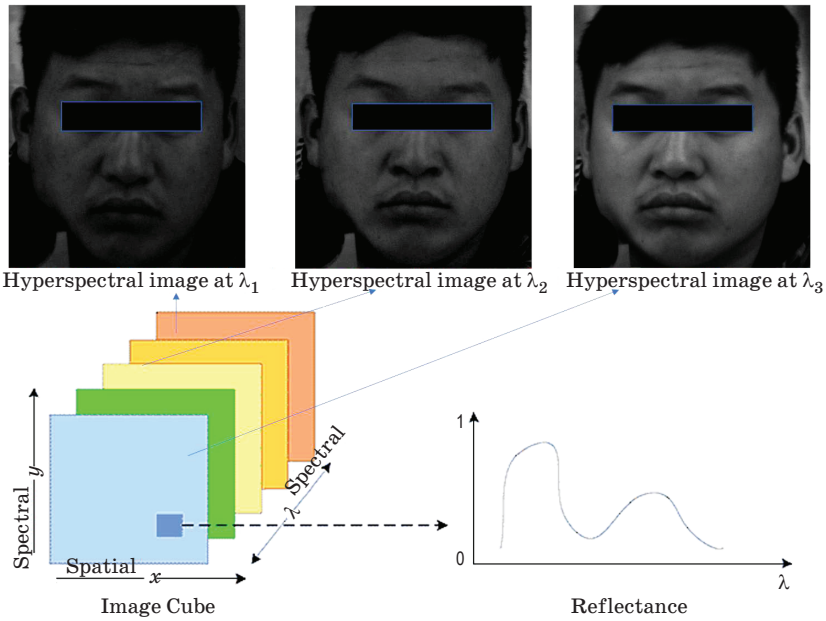

Fig. 1. Image examples and reflectivity of hyperspectral images at different wavelengths (λ).

baseline heart rate so as to judge whether it is under physical stress based on the change rate. As a result, real-time monitoring of physical stress is challenging because background data (especially the baseline HR) are required as a reference.

In this work, the physical stress recognition algorithm is constructed by extracting changes in facial muscle from real-time spectral signal. In response to the above problems, a model of facial muscle activity detection (FMAD) algorithm model is proposed. The main contributions of this work are as follows: (1) Multispectral imaging technology is used to extract real-time physical stress signals from human face. (2) Signal correlation of multi-subject facial region is obtained through multi-variant correlation method, and ROI with the optimal correlation is selected to build the physical stress detection model. (3) Classification features are extracted by ROI muscle track motion change. (4) Finally, a physical stress detection model is constructed by tracking the motion signal to realize contactless physical stress recognition without background data of participants or baseline state information.

The remainder of this paper is organized as follows. Section 2 describes the experimental settings during MSI data acquisition. Section 3 introduces the algorithm model. Section 4 presents the analysis of the results. Section 5 provides a discussion and draws conclusions.

2. ACQUISITION OF PHYSICAL STRESS DATA

2.1. Subjects recruitment

The participants were mainly recruited by posting ads in a newspaper. A total of 37 healthy volunteers and representing both genders participated in the experimental trials. The participants fell in the age group of 20–45 years with a mean age of 27 years and a standard deviation of 10.17. All the participants provided their written informed consent to participate in this study. Among the 37 participant data, 25 will be used for algorithm training and the other 12 for testing.

2.2. Experimental protocol and acquisition set-up

A visible and near-infrared multispectral imaging system covering the spectral wavelengths of 450–800 nm was used (we choose the orange light as ROI band with high signal to noise ratio and high sensitivity). It consists of a Tamron lens, a Brimrose AOTF imaging spectrograph, and a computer. The area CCD array detector of the camera (BM-141GE camera, Japan) has 1392(h)×1040(v) active pixels, and the spectral resolution is 2 nm. MATLAB and BAOTFIS software were used for data acquisition and analysis.

All the experiments performed in this study were conducted following more or less these three main

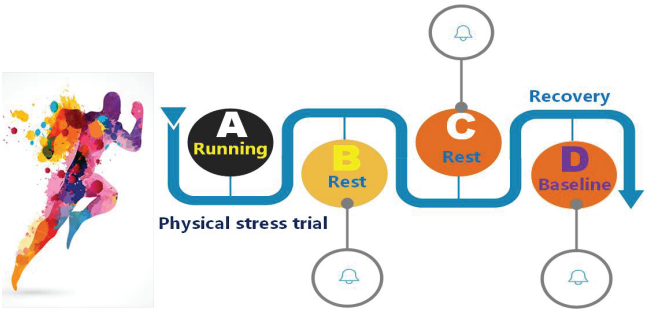

Fig. 2. Timeline of the experiment.

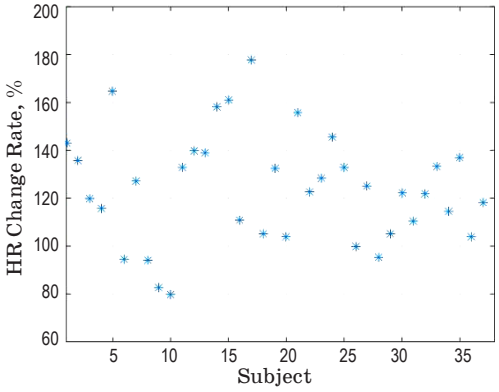

Fig. 3. Changes in HR among the participants after PS.

steps: firstly, the participants were requested to wear a chest strap heart monitor (Garmin) and a finger probe (Miroxi) to measure their HR. Secondly, the participants were led to a well illuminated room where they sat down comfortably. A rest time was given to allow the participants to settle in their new environment. Thirdly, a physical stressors (running) will be given to the participants, followed by a recovery period until the baseline. Figure 2 presents a detailed overview of the experiment design. Figure 3 displays the ground truth results after the test (HR). The participants showed significant increases in heart rate after the PS tests, thereby indicating that our experiments and stressor succeeded in inducing stress.

3. METHODOLOGY FOR PHYSICAL STRESS DETECTION

As mentioned in Introduction, in order to solve the problems in extraction of physical stress signals, we propose a FMAD algorithm, and the physical principle is: changes (or jitter) of facial muscles under physical stress are significantly different from baseline states. In order to extract the muscle changes, the main steps of the algorithm can be described in Fig. 4. Firstly, multispectral images of subjects were obtained during the experiment. Then, the facial signal was extracted and denoised from MSI. After-

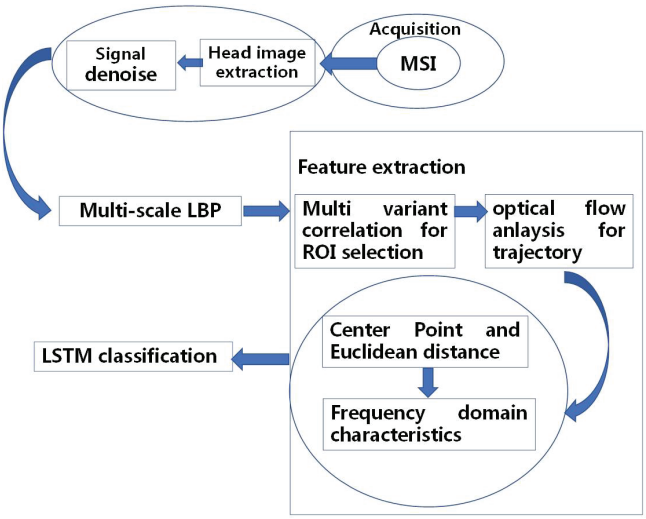

Fig. 4. Main steps of this study.

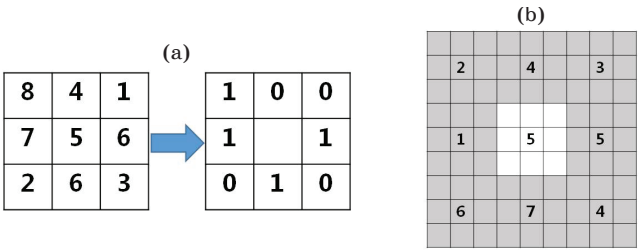

Fig. 5. (a) Original LBP of 3×3, (b) multi-scale LBP of 3×3.

wards, facial ROI under physical stress was selected through the multi-variant correlation method. After obtaining ROI, local binary patterns (LBP) and optical flow algorithms were used to track the motion trajectories of the feature points in the ROI region and extract the motion features from these motion trajectories. Moreover, physical stress and baseline were classified by long short-term memory (LSTM) algorithm. Finally, the contactless physical stress recognition model without background data of participants or baseline state information was constructed.

3.1. Signal denoise for MSI

It is efficient and practical to obtain face information through contactless spectral imaging. However, noise has always been a problem in the industry. The systematic error and noise caused by scattering and path effect are large in the experimental process, which makes the acquisition of pressure features difficult. In the meantime, external interference can also affect data. These problems cannot be solved in experiment or external environment, and the goal of non-contact and non-intervention cannot be realized. To this end, in order to reduce the influence of noise on the algorithm, the feature points are extracted through LBP algorithm model as a reference in de-noising.

The commonly used median filtering, which can filter the noise and protect the edge information of the image from blur, was selected to filter the face image. 4 times 4 size sliding window traversed the image to filter and remove the noise so that the image becomes smoother for the subsequent processing. Afterwards, the feature points of face as a reference can also effectively suppress the effect of noise on image. Therefore, face image is conducted with multi-scale LBP feature processing. Multi-scale LBP features can describe local and global features of an image. The larger the image, the greater the scale. Our image pixel is 1392×1040 size, so we select the multi-scale LBP feature with the scale of 4 for processing.

Multi-block local binary patterns (MB-LBPs) were used to extract face feature points in order to prevent noise from affecting the quality of the face image. As shown in Fig. 5a, the original LBP operator is defined in the neighborhood of pixel 3×3 size. The gray values of eight adjacent pixels are compared with the pixel values in the center of neighborhood by using the neighborhood central pixel as the threshold value. If the surrounding pixels are larger than the central pixel, the location of the pixel point is marked as 1, otherwise 0. In this way, eight points in the neighborhood can be compared to produce an eight-digit binary number. The eight-digit binary number is arranged to form a binary number, which is LBP value of the central pixel. MB-LBP is an extension of basic LBP. An appropriate scale is selected to divide the image area into multiple sub-area blocks, which are further divided into small areas. The LBP feature, namely, MB-LBP is obtained by comparing the gray value of the current small area with that of the surrounding small areas. As shown in Fig. 5b, this area block is 9×9 size, which is divided into 9 small areas with the size of 3×3 size. The value is the average grey value of each small area, which is further compared. MB-LBP not only improves the fast extraction of facial information, but also enhances the robustness to noise. The degree of facial information extraction varies with different scales of MB-LBP. Through multiple experiments, we employ 4 times 4 size MB-LBP to extract and filter the facial signal.

3.2. Multi-subject correlation for ROI selection

After achieving the denoised signal, we analyzed the face signal in depth. It is necessary to identify the ROI before further identifying physical stress. This work aims to find out which parts of face are similar to each other in different participants under physical stress, and the feature signals with high similarity can be used as our target signals. By relating the target signals with the stress matching, the target

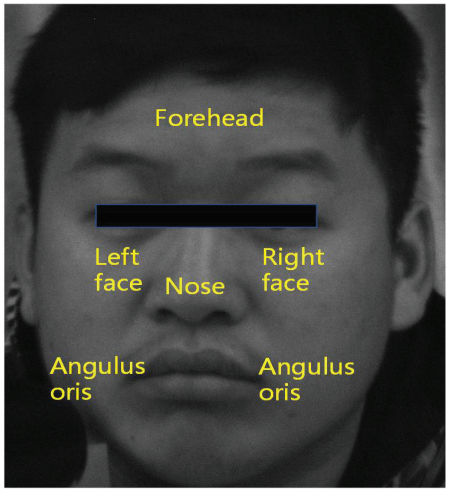

Fig. 6. Possible ROI positions of face.

signal with good correlation is taken as the research object to eliminate the dependence on the baseline data in the conventional approach.

Firstly, the areas sensitive to motion were defined as different objects as possible ROIs, such as left angulus oris, right angulus oris, nose, forehead, left face and right face (Fig. 6). Therefore, we analyze the areas of the facial signals that are sensitive to PS and have a favorable inter-correlation. However, this sensitivity must be built on all participants. That is, the ROI signals of all participants must be sensitive to PS and have robust correlation. In constructing PS recognition system (without baseline data), the general mode of ROI response to PS is crucial. Many previous studies have not systematically studied the choice of ROI, especially the comprehensive analysis of multi-subject signals. Therefore, we must investigate their correlation in this study. Simultaneously, only ROI signals with robust correlation can match the ground truth when the PS recognition system is applied to humans. Unlike the Pearson coefficient, the number of objects that we must build is greater than 2 (our participants are more than 2). The Pearson coefficient can only calculate the correlation between two sets of data; therefore, we utilize a multi-variant correlation method [53–54] to analyze the interrelation between facial signals. This method is based on the zero-lag correlation matrix and random matrix theory. Furthermore, this method can effectively detect and characterize spatiotemporal correlation patterns. In particular, the correlation can be constructed for multiple objects. If the number of subjects N is greater than 2, then the correlation among the multi-variant correlation methods can evaluate multiple channel data. This feature is our requirement.

First, we set an equal-time correlation matrix. A measured multiple ROI time series signal is set to $S_i(t)$ ($i = 1, ..., N$). The equal-time correlation matrix C_{ET} is constructed as follows by normalizing the signal

$$\tilde{S}_i(t) = \frac{S_i(t) - \overline{S_t(t)}}{\sigma_i(t)}. \quad (1)$$

Here, σ_i is the standard deviation, and $\bar{S}_t$ is the mean. We then use the Pearson correlation coefficient to analyze the parameters. Lastly, we set C_{ET} as follows:

$$C_{\mathrm{ET}\,ij}(t) = \frac{1}{T}\sum_{t=1}^{T}\tilde{S}_i(t)\tilde{S}_j(t) = \left\langle \tilde{S}_i\tilde{S}_j \right\rangle_t. \quad (2)$$

Here, all calculations are based on time series $t \in [1, T]$. Therefore, the equal-time correlation matrix can be rewritten as

$$C_{\mathrm{ET}} = \frac{1}{T}\tilde{S}\tilde{S}'. \quad (3)$$

Here, $\tilde{S}'$ is the transposition of $\tilde{S}$. The correlation in the structure of S_i and S_j from various participants is included in the bivariate measures. This correlation is further represented by $N(N - 1)/2$, and the independent coefficient matrix $C_{\mathrm{ET}ij}$, which can explain the cross-correlation between the data of specific participants and other participants. The calculation of this method can provide a direct interpretation. The eigenvalues and characteristic matrices of matrix C_{ET} offer a joint probability distribution of the basic process in which the eigenvalues can demonstrate the level of similarity. For an infinitely long time series, if the signal of all ROI participants is unrelated, then the non-diagonal element of matrix C_{ET} will be equal to 0. By contrast, if the signals are completely correlated, then matrix C_{ET} will be equal to 1. Therefore, the level of the correlation between data depends on the size of the maximum eigenvalue of the C_{ET}. In our case, the S_i (ROI) signal of all finitely long random time series is normalized. After normalization, the eigenvalue distribution of the correlation matrix of S_i can be written as follows [55]:

$$P(\lambda) = \frac{Q}{2\pi}\frac{\sqrt{(\lambda_+ - \lambda)(\lambda - \lambda_-)}}{\lambda}. \quad (4)$$

Here, $\lambda \in [\lambda_+, \lambda_-]$ and Q is equal to T/N. Therefore, λ_- and λ_+ can be obtained as follows:

$$\lambda_\pm(Q) = 1 + \frac{1}{Q} \pm \frac{2}{\sqrt{Q}}. \quad (5)$$

In the signal of all the participants, C_{ET} represents the correlation of each datum. We must only calculate the largest eigenvalue and compare it with λ_+, which can estimate maximum random correlations. If the maximum eigenvalue is larger than that of λ_+, then the description has a certain similarity and correlation. The correlation is inexistent

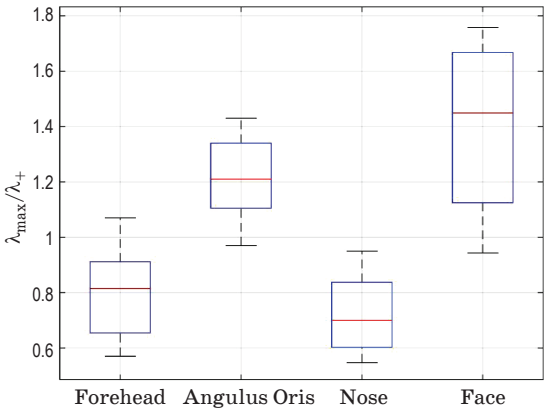

Fig. 7. The normalized maximum eigen value of feature in each running window of the PS data. The test time is 95 seconds, and the test areas are forehead, face, angulus oris and nose.

in the signal data. Therefore, we set the signals of the different participants into the model to analyze whether a correlation exists. The obtained signal from the facial area is regarded as our ROI to achieve PS recognition without background data (baseline status).

We calculated the equal-time signals for 25 participants (for training) through the multi-variant correlation method. Our target time interval after completing a movement is 95 s. The running-window method is used to divide the entire data recording into many adjacent segments. We set the time precision to average the signals as 0.5 s considering the time and time-interval variation precision of signal. The length of the running-window method is set to 13 s. Figure 7 shows the similarity of multi-Subject signals at various parts of the face under physical stress (25 participants). Among the 25 participants, all parts of their faces show multi-subject similarity in feature to different degrees under strong stimulation of physical stress. However, multi-subject similarity of face is the most obvious and continuous, and it is exactly the ROI signal we need. Therefore, we choose the left and right faces as our ROI.

3.3. Motion feature extraction

Face signal was selected on image as ROI. Changes in ROI region were tracked through Lucas-Kandae optical flow. Lucas-Kandae optical flow is a two-frame differential optical flow estimation algorithm. The algorithm assumes that the brightness of the tracked object remains basically constant and the motion is slow relative to frame rate, which is reflected as continuous derivation in mathematics. The algorithm calculates the movement of two frames in each pixel point from time t to $t + \alpha t$. It is Taylor series based on image signals. This method is called difference which uses partial derivatives for space and time coordinates. The image constraint equation can be written as

$$\mathrm{I}(x, y, z, t) = I(x + \delta x, y + \delta y, z + \delta z, t + \delta t), \quad (6)$$

where $I(x, y, z, t)$ is voxel at (x, y, z, t). The movement is assumed to be small enough, and Taylor Formula is used for image constraint equation. We can get

$$\mathrm{I}(x + \delta x, y + \delta y, z + \delta z, t + \delta t) = I(x, y, z, t) + \\ + \frac{\partial I}{\partial x}\delta x + \frac{\partial I}{\partial y}\delta y + \frac{\partial I}{\partial z}\delta z + \frac{\partial I}{\partial t}\delta t + \mathrm{H.O.T.} \quad (7)$$

From this equation we can get

$$\frac{\partial I}{\partial x}V_x + \frac{\partial I}{\partial y}V_y + \frac{\partial I}{\partial z}V_z + \frac{\partial I}{\partial t} = 0, \quad (8)$$

where V_x, V_y, V_z are the optical flow vector of x, y, and z. $\partial I/\partial x$, $\partial I/\partial y$, $\partial I/\partial z$, and $\partial I/\partial t$ give the difference of image pixel at (x, y, z, t). Thereby

$$I_x V_x + I_y V_y + I_z V_z = -I_t. \quad (9)$$

The equation can be written as $\nabla I^T \times \vec{V} = \nabla I^T$. Assume that flow (V_x, V_y, V_z) is a constant in a small window with the size of $m^3 (m > 1)$. The equation can be derived from the pixel group

$$\mathrm{A}\vec{V} = -b. \quad (10)$$

In order to solve the over determination problem, the least square method is used to solve the optical flow equation, and the movement position of the optical flow is obtained, which is the coordinate information of the region to be tracked in the next frame.

We chose three points randomly in the selected ROI and calculated the motion trajectories S_1, S_2, S_3 of the three points by using the optical flow method

$$S_1 = \left[\left(x_1^a, y_1^a\right), \ldots, \left(x_r^a, y_r^a\right), \ldots, \left(x_R^a, y_R^a\right)\right], \quad (11)$$
$$r = 1, 2, 3, \ldots, R,$$

$$S_2 = \left[\left(x_1^b, y_1^b\right), \ldots, \left(x_r^b, y_r^b\right), \ldots, \left(x_R^b, y_R^b\right)\right], \quad (12)$$
$$r = 1, 2, 3, \ldots, R,$$

$$S_3 = \left[\left(x_1^c, y_1^c\right), \ldots, \left(x_r^c, y_r^c\right), \ldots, \left(x_R^c, y_R^c\right)\right], \quad (13)$$
$$r = 1, 2, 3, \ldots, R,$$

$$S_0 = \left\{\frac{\left(x_1^a + x_1^b + x_1^c\right)}{3}, \frac{\left(y_1^a + y_1^b + y_1^c\right)}{3}\right\}, \quad (14)$$

where x and y are the positions of the points, a, b, and c are the three feature points. For example, (x_1^a, y_1^a) is the position of the first frame of the first feature point, and so forth. R is the number of frames, and there is a total of R frames. We select the central point of three points in the ROI region of the first frame as the fixed reference point S_0.

Through these tracks, we can know the movement of the participant's facial regions. According to the three feature points, the Euclidean distance between the three feature points and the fixed reference point was calculated, and three groups of feature sequences D_1, D_2, and D_3 were obtained. Finally, the average value of these three distance feature sequences is obtained as the final feature sequence D, which is time-continuous

$$D_i = S_i - S_{02}, \quad i = 1, 2, 3, \tag{15}$$

$$D = \sum_i D_i / 3, \tag{16}$$

where D is the signal output. The high frequency jitter signal in PS state were extracted and conducted with classification training as features in the LSTM model.

4. EXPERIMENTAL RESULTS AND ANALYSIS

Firstly, the signals of 25 participants were trained as training features in the algorithm model. The feature signals were transformed from time domain to frequency domain for analysis. The feature sequences were conducted with Fourier transform, and the time domain is transformed into frequency domain. Figure 8 shows a typical feature case. According to the spectrum of baseline and motion state, it can be seen that there is no obvious peak in the fast Fourier transformation (FFT) diagram in the baseline state, and the waveforms are all disorder and irregular. However, there is an obvious peak value at 1.5 Hz on the FFT diagram in moving state. In the meantime, we summarized the peak ranges of all participants (Fig. 9) and found that their muscle jitter high frequency ranges were higher than 1 Hz. The peak frequency of muscle movement varies from person to person in PS state. However, this shows that muscle motion feature D is sensitive to PS. Therefore, we put the facial muscle jitter signal D as the final feature signal of FMAD algorithm into the LSTM model to train our feature signal classification model and realize the final baseline and PS classification detection model.

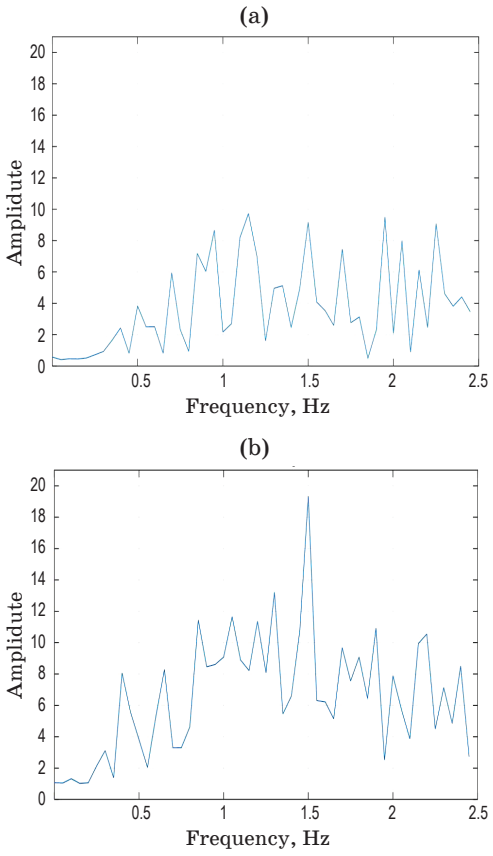

Fig. 8. Typical feature signal spectrum (using FFT). (a) Baseline spectrum, (b) PS spectrum.

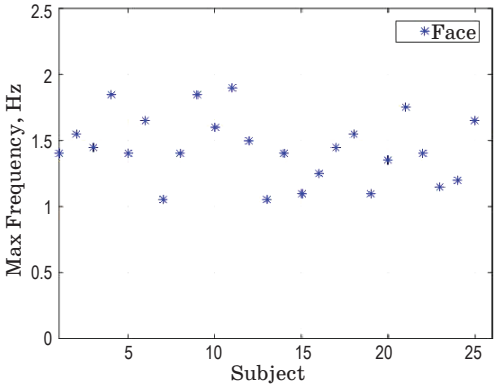

Fig. 9. Peak frequency of feature signal motion.

The extracted feature signal is sensitive to PS, which lays a foundation for classification. The feature signal is trained as input in the LSTM model. The training platforms are Python and tensorflow. The following figure shows that we built a classification network based on LSTM through tensorflow. By taking the frequency information as input, eight LSTM cell units were set. The learning rate is 0.003, and batch size is 30. The output is classified into PS state and baseline state. The data of the remaining 12 participants are taken as testing. The test was completed on tensorflow that can be visualized.

Accuracy of other famous algorithms

Algorithm	Accuracy, %
Support Vector Machine	32
Competitive adaptive reweighted sampling	26
Bayes	41
k-Nearest Neighbor	19
Back Propagation	20
Ensemble Learning	28

The classification accuracy of FMAD algorithm is up to 75%. By comparing with other famous classifiers (Table), the results show that our algorithm has obvious advantages and high accuracy.

5. DISCUSSION

This paper presented a physical stress recognition algorithm based on multispectral real-time imaging technology. Our algorithm can classify physical stress state and baseline state of human body. As far as the authors know, this is the first time in the field to identify human physical stress through multispectral imaging technology. Our algorithm extracts facial muscle motion parameters by multispectral imaging and classifies physical stress state and baseline state of human body according to the changes of facial muscle motion state. Moreover, the algorithm can recognize physical stress without background data or baseline data as reference.

The movement of face muscle will change under stress. The algorithm foundation is constructed according to this physiological feature. After obtaining the real-time facial spectral signal by multispectral imaging, we first used median filtering method for image denoising and smoothing. Afterwards, the face images were conducted with multi-scale LBP feature processing because we need the feature points of face as a reference. This can also effectively suppress the effect of noise on images. In the meantime, multi-scale LBP features can describe local and global features of images. After the feature points were obtained, we used multi-subject similarity correlation method to systematically analyze the spectral signals of each part on face and determined cheek as our ROI. Our selection of ROI is more systematic than previous studies. In order to realize the contactless PS recognition without background data, we extracted the feature of muscle motion track at ROI by using optical flow method. The physical stress recognition without interference or background data is realized through LSTM algorithm model training classification.

Our future work is quite heavy because there are still many shortcomings and goals to be overcome or achieved. Firstly, the experiment range needs to be expanded, and the current number of participants in the experiment can be increased to obtain larger samples. Secondly, although the multispectral imaging realizes the acquisition of real-time data, the real-time tracking and extracting algorithm of ROI will be the key point in the next step. The recognition rate of 75% for the application in the industry field is not good enough. The accuracy of recognition should be improved further in the next step. Thirdly, the data were collected in laboratory environment. The future work will focus on the expansion of experimental environment, so that our research and development algorithm can better combine with industrial application. In the meantime, further quantification of physical stress can quantify physical stress in a hierarchical manner, which is challenging. However, this will lay a foundation for the next industrial application. For example, we plan to install the imaging system in cabs to extract the PS information of drivers in real time, which can provide effective information for quantifying their fatigue degree.

ACKNOWLEDGMENT

The work was carried out with financial support of National Natural Science Foundation of China (61741507), Science Foundation for Young Scientists of Jiangxi Province under grant 20171BAB212019 and Science and Technology Project Foundation of the Education Department of Jiangxi Province under grant GJJ150798. Dr Kan Hong and Dr Guodong Liu are corresponding authors.

REFERENCE

1. *Lederbogen F., Baranyai R., Gilles M.* Effect of mental and physical stress on platelet activation markers in depressed patients and healthy subjects: A pilot study // Psychiatry Research. 2004. V. 127. № 1. P. 55–64.
2. *Otto M.* Physical stress and bacterial colonization // Fems Microbiology Reviews. 2014. V. 38. № 6. P. 1140–1250.
3. *Tripathi R.K.* Effect of Withania somnifera on physical and cardiovascular performance induced by physical stress in healthy human volunteers // International J. Basic & Clinical Pharmacology. 2016. V. 1. № 1. P. 2279–2289.
4. *Amita M.P.* Comparison of anthropometric parameters and blood pressure changes in response to physical stress test in normotensive subjects with or without family history of hypertension // J. Physiol. Pharmacol. 2016. V. 60. № 2. P. 208–212.
5. *Ktedalen O.* The influence of prolonged physical stress on gastric juice components in healthy man // Scandinavian J. Gastroenterology. 1988. V. 23. № 9. P. 1132–1136.
6. *Wallen N.H.* Effects of mental and physical stress on platelet function in patients with stable angina pectoris and healthy controls // European Heart J. 1997. V. 18. № 1. P. 807–815.
7. *Michael T.* Impact of mental and physical stress on blood pressure and pulse pressure under normobaric versus hypoxic conditions // Plos One. 2014. V. 9. № 5. P. e89005.
8. *Irfan M.* Physical stress may result in growth suppression and pubertal delay in working boys // Iranian J. Medical Hypotheses & Ideas. 2011. V. 5. № 1. P. 35–39.

9. *Gillan W.* Correlations among stress, physical activity and nutrition: School employee health behavior // The ICHPER-SD J. Research in Health. 2013. № 8. P. 55–60.

10. *Mizuno M.* Prenatal programming of hypertension induces sympathetic overactivity in response to physical stress // Hypertension. 2013. V. 61. № 1. P. 180.

11. *Taylor A.H.* Stress, fatigue, health, and risk of road traffic accidents among professional drivers: The contribution of physical inactivity // Annual Review of Public Health. 2006. V. 27. № 1. P. 371.

12. Natrual Tech: The Adrenal Stress Profile. http: // www.natratech.com /Products / saliva_test.htm. Accessed 7 March 2015.

13. *Read G.F.* Immunoassays of steroids in saliva // Steroid Biochem. 1985. V. 22. № 33. P. 437–438.

14. *Nardelli M.* Recognizing emotions induced by affective sounds through heart rate variability // IEEE Trans. Affective Computing. 2015. V. 6. № 4. P. 385–394.

15. *Cook A.J.* Open platform, eight-channel, portable bio-potential and activity data logger for wearable medical device development // Electron. Lett. 2015. V. 51. № 21. P. 1641–1643.

16. *Kozel F.A.* Detecting deception using functional agnetic resonance imaging // Biol. Psychiatry. 2005. V. 58. P. 605–613.

17. *Bhatt S.* Lying about facial recognition: An fMRI study // Brain Cognit. 2009. V. 69. P. 382–390.

18. *Ebisch S.J.* Mother and child in synchrony: Thermal facial imprints of autonomic contagion // Thermology International. 2012. V. 22. P. 121–129.

19. *Ioannou S.* The autonomic signature of guilt in children: A thermal infrared imaging study // Plos One. 2013. V. 8. P. 1–11.

20. *Puri C.* Stress-cam: Non-contact measurement of user's emotional states through thermal imaging // Proc. 2005 ACM Conf. Human Factorsin Computing Systems. 2005. V. 2. P. 1725–1728.

21. *Garbey M.* Contact-free measurement of cardiac pulse base on the analyses of thermal imagery // IEEE Trans. Biomedical Engineering. 2007. V. 54. P. 1418–1426.

22. *HaoYu W.* Eulerian video magnification for revealing subtle changes in the world // ACM Trans. 2012. V. 31. № 4. P. 1–8.

23. *Pavlidis I.* Interacting with human physiology // Computer Vision & Image Understanding. 2007. V. 108. P. 150–170.

24. *Pavlidis I.* Human behavior: Seeing through the face of deception // Nature. 2002. V. 415. № 6867. P. 35–36.

25. *Pavlidis I.* Continuous physiological monitoring // Proc. 25th Annual Intern. Conf. IEEEEMBS Cancun. 2003. P. 17–21.

26. *Pavlidis I.* Thermal image analysis for anxiety detection // Proc. 2001 IEEE Intern. Conf. Image Proc. 2001. V. 2. P. 315–318.

27. *Cross C.B.* Thermal imaging to detect physiological indicators of stress in humans // SPIE Defense Security & Sensing. 2013. V. 3. № 1. P. 8705–8711.

28. *Boethig D.* Physical stress testing of bovine jugular veins using magnetic resonance imaging, echocardiography and electrical velocimetry // Interactive Cardiovascular & Thoracic Surgery. 2010. V. 10. № 6. P. 877.

29. *Slobounov S.M.* Alteration of brain functional network at rest and in response to YMCA physical stress test in concussed athletes: RsFMRI study // Neuroimage. 2011. V. 55. № 4. P. 1716.

30. *Ji Q.* Real-time nonintrusive monitoring and prediction of driver fatigue // IEEE Trans. Vehicular Technol. 2004. V. 53. № 4. P. 1052–1068.

31. *Tayibnapis I.R.* A novel driver fatigue monitoring using optical imaging of face on safe driving system // Intern. Conf. Control. 2017. V. 1. № 1. P. 115–120.

32. *Yangon Q.* A novel real-time face tracking algorithm for detection of driver fatigue // Third Intern. Symp. Intelligent Information Technology & Security Informatics. 2010. V. 1. P. 671–676.

33. *Hong K.* Classification of the emotional stress and physical stress using signal magnification and canonical correlation analysis // Pattern Recognition. 2018. V. 77. № 1. P. 140–149.

34. *Alioua N.* Driver's fatigue detection based on yawning extraction // Intern. J. Vehicular Technology. 2014. V. 1. P. 1–7.

35. *Sacco M.* Driver fatigue monitoring system using support vector machines // 2012 Fifth Intern. Symp. Communications Control and Signal Proc. 2012. P. 1–5.

36. *Liu A.* A practical driver fatigue detection algorithm based on eye state // Proc. Asia Pacific Conf. Postgraduate Research in Microelectronics and Electronics. Shanghai, China. 2010.

37. *Liu D.* Drowsiness detection based on eyelid movement // Proc. 2nd Intern. Workshop on Education Technology and Computer Science. Wuhan, China. 2010.

38. *Jimenez-Pinto J.* Face salient points and eyes tracking for robust drowsiness detection // Robotica. 2012. V. 30. № 5. P. 105–115.

39. *Irani R.* Contactless measurement of muscles fatigue by tracking facial feature points in a video // IEEE Intern. Conf. Image Proc. 2014. V. 12. № 1. P. 127–135.

40. *Mohammad A.* Facial video-based detection of physical fatigue for maximal muscle activity // IET Computer Vision. 2016. V. 10. № 4. P. 323–329.

41. *Hong K.* Real time stress assessment using thermal imaging // The Visual Computer. 2015. V. 10. P. 1–9.

42. *Hong K.* Classification of emotional stress and physical stress using facial image feature // JOT. 2016. V. 83. № 8. P. 1–10.

43. *El Masry G.* Quality classification of cooked, sliced turkey hams using NIR hyperspectral imaging system // J. Food Eng. 2011. V. 103. P. 333–344.

44. *Xie C.* Study of detection of SPAD value in tomato leaves stressed by grey mold based on hyperspectral technique // Spectroscopy & Spectral Analysis. 2012. V. 32. P. 3324–3328.

45. *Noora N.* Detecting field cancerization using a hyperspectral imaging system laser surg med // Scientific Reports. 2013. V. 45. P. 410–417.

46. *Richard M.* Consistency of measurements of wavelength position from hyperspectral imagery: Use of the ferric iron crystal field absorption at similar to 900 nm as an indicator of mineralogy // IEEE T. Geosci. Remote. 2014. V. 52. P. 2843–2857.

47. *Michael D.* New ways to extract archaeological information from hyperspectral pixels // J. Archaeol. Sci. 2014. V. 52. P. 84–96.

48. *Chuanqi Xie.* Detection of early blight and lateb light diseases on tomato leaves using hyperspectral imaging // Scientific Reports. 2015. V. 5. P. 16564.

49. *Chen T.* Assessment of tissue blood perfusion in-vitro using hyperspectral and thermal imaging techniques // 5th Intern. Conf. Bioinformatics and Biomedical Eng. 2011. V. 1. P. 1022–1030.

50. *Chen T., Yuen P., Hong K.* Remote sensing of stress using electro-optics imaging technique // Proc. SPIE. 2009. V. 7486. P. 601–612.

51. *Yuen P., Chen T., Hong K.* Remote detection of stress using hyperspectral imaging technique // Proc. 3rd Intern. Conf. Crime Detection and Prevention ICDP. 2009. V. 1. 12. P. 500–512.

52. *Veronika E.* Exploring the use of thermal infrared imaging in human stress research // J. Plos One. 2014. V. 9. № 3. P. 125–136.

53. *Muller M.* A multivariate approach to correlation analysis based on random matrix theory // Seizure Prediction in Epilepsy: From Basic Mechanisms to Clinical Applications B. / Eds. by Schelter J., Timmer A., and Bonhage S. N.Y., USA: Wiley, 2008. P. 209–226.

54. *Wanhui W.* Emotion recognition based on multi-variant correlation of physiological signals // IEEE Trans. Affective Computing. 2014. V. 5. № 2. P. 40–60.

55. *Edelman A.* Eigenvalues and condition numbers of random matrices // SIAM J. Matrix Anal. Appl. 1988. V. 9. № 4. P. 543–560.